Origin of the x-ray-absorption fine structure in photon-stimulated ion desorption from Si-adsorbate systems

R. McGrath
Interdisciplinary Research Centre in Surface Science and Department of Physics, Liverpool University, P.O. Box 147, Liverpool L69 3BX, United Kingdom

I. T. McGovern
Department of Pure and Applied Physics, Trinity College, Dublin 2, Ireland

D. R. Warburton, D. Purdie, C. A. Muryn, N. S. Prakash, P. L. Wincott, and G. Thornton
Interdisciplinary Research Centre in Surface Science and Department of Chemistry, Manchester University, Manchester M13 9PL, United Kingdom

D. S-L. Law and D. Norman
Science and Engineering Research Council, Daresbury Laboratory, Warrington WA4 4AD, United Kingdom
(Received 10 September 1991)

There is no general agreement on whether photon-stimulated ion desorption (PSID) extended and near-edge x-ray-absorption fine structure (EXAFS and NEXAFS) can provide surface structural information. To address this question, we have monitored the H^+-ion yield from Si(100)2×1-H, Si(111)7×7-H_2O, and Si(111)7×7-H at the substrate Si *K* edge and the Cl^+-ion yield for the systems Si(100)2×1-Cl and Si(111)7×7-Cl at both the substrate Si *K* edge and adsorbate Cl *K* edge. Moreover, we reassess our previously published Si *K*-edge H^+-ion yield data from the Si(100)2×1-H_2O system. The EXAFS in the ion yield spectra is analyzed with a view to clarifying the physical processes determining the ion yield. At the substrate Si *K* edge, the similarity of near-neighbor distances and coordination numbers to bulk values in all the systems studied indicates that the ion yield at this edge is dominated by x-ray-induced electron-stimulated desorption. This is corroborated by NEXAFS data at the same absorption edge. For Si(100)2×1-Cl and Si(111)7×7-Cl the Cl^+-ion yield at the Cl *K* edge produces EXAFS and NEXAFS spectra identical to those recorded using Auger-electron yield, indicating the likely desorption mechanism to be a Knotek-Feibelman intra-atomic Auger process. The implications of these findings for PSID EXAFS, and NEXAFS are discussed.

I. INTRODUCTION

Surface extended x-ray absorption (SEXAFS) and near-edge x-ray absorption (NEXAFS) are established techniques for the determination of short-range surface structure.[1] One major disadvantage with both techniques (in comparison with other structural probes such as low-energy electron diffraction or surface x-ray diffraction) is that they are limited to studying the structure around *adsorbate* atoms: here the adsorbate is the "central atom" where the photoabsorption event occurs and the substrate and other adsorbate atoms are the backscatterers. If a substrate atom is photoionized, the EXAFS information is dominated by the signal coming from the bulk absorption events. This means that it is not possible to study clean surfaces with the usual variants of the SEXAFS and NEXAFS technique.

There have been two distinct attempts to move beyond this situation. One was a study of the clean surface of Si by monitoring the yield of Si *LVV* Auger electrons of energy (~92 eV) close to the minimum in the mean free path and hence originating within 5 Å of the surface.[2] This provided NEXAFS information, but because the photoelectron peak swept through the kinetic-energy window of the detector, the data range was limited to ≤92 eV—too short for useful EXAFS information.

A second approach has been to study the local geometry about a surface *substrate* atom in the presence of an adsorbate using the yield of desorbed adsorbate ions above a *substrate edge*. The EXAFS and NEXAFS in the yield of desorbed ions should probe the local geometry of the substrate atom to which the desorbed ion was bonded, *provided that* the ion desorption event is directly related to the substrate *surface* ionization rather than to the bulk.

This condition is satisfied if the dominant desorption mechanism is that described by Knotek and Feibelman (KF).[3,4] This mechanism was originally proposed to explain the increase in O^+ electron-stimulated desorption (ESD) yields from TiO_2, V_2O_5, and WO_3 when the incident electron energy is large enough to ionize the metal atoms in the sample. Extending this mechanism to an adsorbate-substrate system, the inner shell hole on a substrate surface atom is filled by an inter-atomic Auger process; this results in at least two holes in the valence levels of the adsorbate, thus breaking the bond of the adsorbate

complex. The adsorbate is desorbed as a positively charged ion due to reversal of the sign of the Madelung potential—the so-called Coulomb explosion. In this KF mechanism, the desorption of an adsorbed atom may proceed only via photon absorption at the substrate atom to which the adsorbate is directly bonded; the range of the wave-function overlap ensures that more distant atoms cannot be involved.[5] As the desorption follows the photoionization event, it is the undisturbed structure which causes the EXAFS and the adsorbate atom should be visible as a backscatterer prior to its desorption. Photon-stimulated ion desorption (PSID) should provide SEXAFS and NEXAFS signal with a very low background and thus large edge jump.

The first PSID EXAFS experiment reported by Jaeger *et al.*,[6] involved the study of Mo(100)-O in which O was thought to be bonded in an ionic form. Monitoring the yield of O^+ ions above the Mo $L_1(2s)$ edge, it was found that the SEXAFS was dominated by a Mo-Mo first shell, with a bond distance equal to that in bulk Mo. The coordination number of this shell was, however, half that of the bulk [recorded in total electron yield (TEY)] leading to the conclusion that the data were surface specific and that the KF mechanism was dominant. Due to overlapping Mo $L_{2,3}$ edges in the low-k region of the spectrum where O backscattering might be expected, an O-Mo shell was not isolated. The conclusion was that the desorbing O atoms were bonded without inducing major surface reconstruction.

Since the PSID EXAFS study of Jaeger *et al.*, there have also been several NEXAFS studies of Si-adsorbate systems at the Si $2p$ edge which indicated that a KF mechanism dominated.[7–10] However, in other studies a competing desorption mechanism giving only bulk information has been found to dominate. The mechanism usually invoked to explain ESD is that of Menzel, Gomer, and Redhead (MGR).[11] In this model desorption occurs following a Franck-Condon transition to an antibonding, metastable or ionic state of the complex; these excited states normally involve only valence-level excitations. Thus MGR events could arise at the surface from photoexcitation of bulk atoms and subsequent secondary electron migration to the surface. This mechanism, known as x-ray-induced electron-stimulated desorption (XESD), has been found to contribute substantially to or to dominate the ion yield in a number of *substrate* edge studies,[12–15] though the dominance of the XESD mechanism in the work of Refs. 12–14 has since been questioned.[16] In our previous study of the H^+ yield from Si(100)2×1-H_2O at the Si K edge,[17] the bond lengths obtained were close to those of bulk values; however, a KF mechanism was inferred, because the PSID edge jump was different from that in TEY. The assumption was that the XESD above a substrate absorption edge should mirror the TEY. Subsequently Menzel[18] questioned whether this was a sufficient criterion, and this led us to show that the edge jumps in TEY and XESD are not necessarily similar, being, in fact, a complex function of the electron distribution $N(E)$ and the ion desorption cross section $\phi(E)$.[19] In the light of this evidence, we include here a reassessment of the Si(100)2×1-H_2O data.

In view of the uncertain situation, Menzel[18] has called for further studies, especially of systems where both the adsorbate and substrate core levels are accessible and thus the adsorbate-substrate distance may be determined by conventional SEXAFS techniques. In addition, this offers the possibility of PSID at the *adsorbate* edge and although several adequate detection mechanisms exist for SEXAFS and NEXAFS at this edge, there is intrinsic interest in ion-yield measurements at such an edge related to the study of minority absorption sites. In one study of adsorbate edge excitation, a KF mechanism has been found to dominate.[20] There the desorption process proceeds via an intra-atomic Auger process leading to a Coulomb explosion. Notably, this allowed a measurement of the C 1s NEXAFS in CO adsorbed on Ru(001), a measurement not possible with Auger yield because of an overlapping photoelectron peak. In other systems, though, the ion yield has been found to arise from a mixture of PSID and XESD (Refs. 12 and 13) or from desorption due to higher excitations (core shakeup and shakeoff).[20–22] In these cases the ion yield deviates from the absorption coefficient as measured by conventional Auger yield.

To summarize, in this work we have monitored PSID EXAFS and NEXAFS for a number of Si-adsorbate systems to determine whether the ion desorption is dominated by surface or bulk processes. Chlorine was chosen as the adsorbate for which both adsorbate and substrate edges could be studied. Moreover, Cl should be a "visible" backscatterer as its backscattering amplitude is much stronger than that of H or O,[23] and the Cl-Si bond length is known to be different from the Si-Si distance in bulk silicon. The systems studied were Si(100)2×1-H_2O, Si(100)2×1-H, Si(111)7×7-H_2O, Si(111)7×7-H, Si(100)2×1-Cl, and Si(111)7×7-Cl.[24] Measurements were made of the H^+ yield at the Si K edge, and of the Cl^+ yield at both Si and Cl K edges. In addition Auger-yield SEXAFS spectra above the Cl K edge were recorded from Si(100)2×1-Cl and Si(111)7×7-Cl for comparison. The structures of all of these systems are relatively well known from a variety of previous studies.[25–38] A comparison of PSID EXAFS results (bond lengths and coordination numbers) with the values calculated for the known adsorption geometry allows the origin of the EXAFS to be determined. The NEXAFS spectra are also qualitatively compared with those from bulk systems and with Auger NEXAFS measurements. These data allow a more complete assessment of the prospects for this technique than has previously been attempted.

II. EXPERIMENTAL AND DATA ANALYSIS DETAILS

Measurements were performed at a base pressure of $<2\times10^{-10}$ Torr, the residual gas being mainly H_2 (partial pressure of $H_2O<5\times10^{-12}$ Torr). All measurements were made at room temperature. The Si(100) and Si(111) crystals were cleaned and ordered using either cycles of 0.5-keV Ar^+-ion bombardment and annealing to 1240 K, or by flash annealing the as-inserted crystal to remove the surface oxide. Auger electron spectroscopy with either a double-pass cylindrical mirror analyzer (CMA) or a re-

tarding field analyzer was used to determine surface cleanliness and low-energy electron diffraction (LEED) was used to determine the surface order.

Water dosing was achieved by exposing the sample at 295 K to the vapor from doubly distilled H_2O, which had been treated with several freeze-thaw cycles to remove impurities. The 2×1 and 7×7 symmetries were maintained up to the saturation H_2O exposures of 2 and 100 L, respectively. On the (100) surface the H_2O dissociates with the adsorption of H and OH on the dimer atoms.[25–27] H_2O adsorption on Si(111) is also dissociative and the adsorption site is thought to be atop.[28,29]

Atomic H dosing was achieved by exposing to research-grade H_2 gas dissociated with a hot tungsten filament ~5 cm from the sample and in line of sight. For Si(100) a dose of 10 L led to the formation of the Si(100)2×1:H monohydride species.[29] Dosing was carried out with the sample at elevated temperature to prevent reaction with H_2O from the residual vacuum.[30] For Si(111)7×7 a dose of 40 L led to the low-coverage monohydride phase as evidenced by the LEED pattern which remained 7×7.[31]

An electrolytic Cl source, consisting of a Ag gauze anode and a Pt foil cathode with an "electrolyte" composition (by mass) of 1% $CdCl_2$ and 99% AgCl (Ref. 39) was used to dose the Si crystals. Ion flux was enhanced by heating the electrolyte pellet with a tungsten filament to 320–370 K, and the sample was maintained at ~570 K during dosing. The dosing was continued until saturation coverages were recorded on both surfaces. In both cases the LEED pattern was unchanged from that of the clean surface.

Desorbed ions were detected using a specially constructed time-of-flight (TOF) detector.[15] This consists of a 1-cm-diam drift tube of length 3 cm, approximately 2 cm from the sample. The drift tube is at a large negative potential ($V_1=-2.2$ keV) so that small differences in the desorption kinetic energies can be neglected (i.e., the ion flight times are solely determined by the applied voltages). The ions are detected using a matched pair of multichannel electron multiplier plates and a 50-Ω coaxial anode, the output of which is connected to a chamber feedthrough via a coaxial cable. The first channel plate is operated at a more negative potential than the drift tube to ensure that electrons photoemitted from the drift tube by fluorescent photons and scattered x rays are not detected, though fluorescent photons directly hitting the channel plates are detected. A schematic diagram of this detector with the associated electronics is shown in Fig. 1.

The ion-yield experiments were carried out on line 6.3 at the Daresbury Laboratory Synchrotron Radiation Source (SRS).[40] The TOF measurements utilize the time structure of the storage ring in single bunch mode (bunch width ~200 ps, orbit time 320 ns). When an ion or photon triggers the detector, the time-to-digital converter is started which counts in 1-ns intervals until stopped by a pulse from the SRS orbit clock. This time interval Δt is recorded in a 512 channel histogramming memory which is incremented by one unit in a channel corresponding to Δt and thus a TOF spectrum is built up. The ion flight

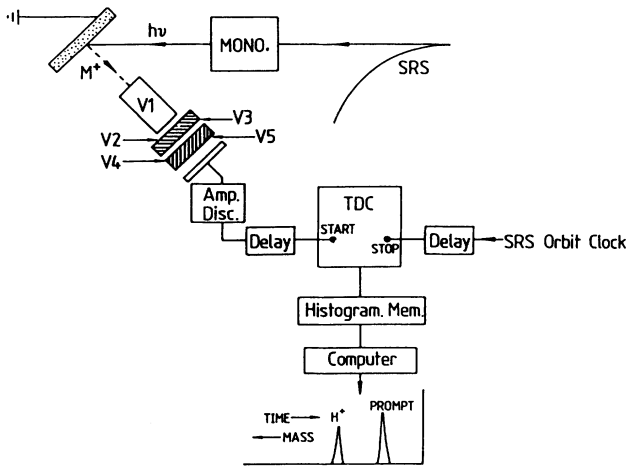

FIG. 1. Schematic diagram of the TOF mass spectrometer and associated electronics. TDC is the time-to-digital converter. The operation is described in the text.

times can thus be measured relative to the prompt peak which is triggered by a fluorescent photon from the sample, which reaches the detector almost immediately. The absolute flight times t_i can thus be measured relative to the prompt pulse at $t=0$; different ion species can be identified using the relation

$$\frac{m_1/q_1}{m_2/q_2}=\left[\frac{t_1}{t_2}\right]^2, \tag{1}$$

where m_1 and m_2 are the masses of two ion species, q_1 and q_2 are their charge, and t_1 and t_2 are their drift times. A typical TOF spectrum from Si(111)7×7-Cl at a photon energy 480 eV above the Cl K edge is shown in Fig. 2.

Ion-yield EXAFS spectra were recorded by monitoring the photon energy-dependent intensity variation of a given peak in the TOF spectrum. The Si K-edge (1839 eV) measurements utilized the InSb(111) crystals ($2d=7.4860$ Å), while the Ge(111) crystals ($2d=6.270\,64$ Å) were used at the Cl K edge (2823 eV). The low ion yields obtained in off-normal emission meant that the experiments were performed with the light at grazing incidence on the sample (20±5°) and normal emission (±5°). The ion-yield signals were flux normalized using the drain current from a 90% transparent Cu mesh as a monitor of the incident intensity. TEY Si K-edge spectra were recorded for use as model bulk Si data for the SEXAFS analysis procedure. For Auger SEXAFS measurements at the Cl K edge, a double-pass CMA (Physical Electronics Inc.) operated in nonretard mode was used with the CMA axis being at 90° to the incident photon beam. The kinetic energy of the analyzer was set to 2363 eV to monitor the Cl KLL Auger electron yield (AEY).

Data reduction and analysis were done using the SRS program library at Daresbury. After normalization to the edge height and subtraction of a smoothly varying polynomial background the normalized oscillatory part of the fine structure $\chi(k)$ was analyzed using the EXCURVE fitting program.[41] Phase shifts were calculated

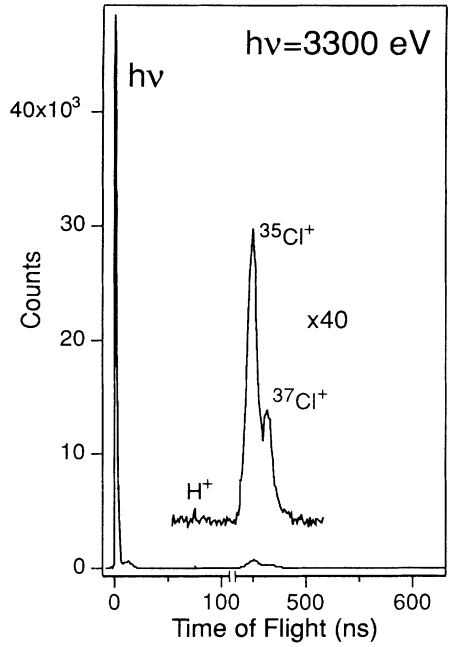

FIG. 2. TOF spectrum recorded from the Si(111)7×7-Cl at 15° x-ray incidence, with ions emitted around normal to the Si(111) substrate being detected. The accumulation time as 10 s. The dominant peak is from fluorescent photons with another fluorescent peak at 12 ns due to an impurity in the exciting beam. As well as the two Cl^+ peaks with flight times of 451 and 465 ns, a small H^+ feature is seen at 76 ns. The abscissa scale break accounts for the Cl^+-ion flight time being greater than the SRS repetition period of 320 ns.

for Si and Cl central atoms and Si and Cl backscatterers and then refined empirically by fitting EXAFS data from the standard compounds bulk Si (TEY data) and $SiCl_4$.[42] Effective coordination numbers were also extracted from the data using model compound values for the other amplitude parameters.

Experimentally determined effective coordination numbers N_j^* were compared with calculated values for the different structural geometries for each system. N_j^* can be calculated for any system from the expression

$$N_j^* = 3 \sum_{i=1}^{N_j} \cos^2\theta_{ij} \ , \tag{2}$$

where θ_{ij} is the angle between the polarization vector **A** and $\mathbf{r}_{ij}$, and N_j is the actual number of atoms in the jth shell. In the case where a given shell consists of more than one bond distance, contributions were weighted according to the scheme introduced by Citrin, Eisenberger, and Rowe.[43] For bond lengths R_1 and R_2 close in distance, and $R_1 < R_2$, the effective coordination number N^* is the sum of contributions from the atoms at R_1 and the atoms at R_2 weighted by $(R_1/R_2)^2$:

$$N^* = N_1^* + \left[\frac{R_1}{R_2}\right]^2 N_2^* \ . \tag{3}$$

The average bond length in this scheme is given by

$$\bar{R} = \alpha R_1 + (1-\alpha) R_2 \ , \tag{4}$$

where $\alpha = N_1^*/N^*$.

III. RESULTS

This section is divided into two parts. In the first part we consider the data taken at the substrate Si K edge. The second section considers the adsorbate Cl K-edge measurements.

A. Si K-edge measurements

Figure 3 shows a comparison of ion-yield data with bulk TEY data for several systems recorded at the Si K edge. Collection times for the ion yield spectra were typically 20 s per point, and the energy step used was 2 eV giving a total collection time of 1–1.5 h per spectrum allowing for dead time. Differences in the quality of the ion-yield data arise mainly from different beam conditions in the storage ring. From the tick marks above the main spectral features, it can be seen that the spectra are qualitatively similar. This would be expected in cases (b)–(e) where the Si-Si surface atoms bond length would not be very much different from the bulk case (2.35 Å). In the case of the Cl adsorbate surfaces it indicates that the Cl-Si bond length (typically 2.00 Å in other compounds) does not give rise to a large modification of the

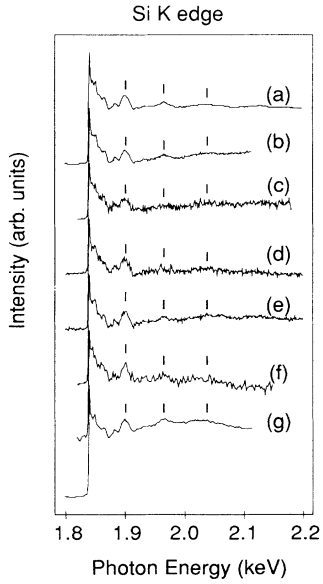

FIG. 3. Comparison of Si K-edge scans at grazing incidence. The spectra have been normalized to the absorption edge height. (a) Bulk Si total electron yield; (b) H^+ yield from Si(1002×1-H_2O; (c) H^+ yield from Si(100)2×1-H; (d) H^+ yield from Si(111)7×7-H_2O; (e) H^+ yield from Si(111)7×7-H; (f) Cl^+ yield from Si(100)2×1-Cl; and (g) Cl^+ yield from Si(111)7×7-Cl. The tick marks above the main EXAFS features are provided as a guide to the eye.

EXAFS.

The EXAFS oscillations were isolated as described in the preceding section. As an example, the background subtracted and edge step normalized EXAFS $\chi(k)$ weighted by k^3 from Si(100)(2×1)-H_2O is shown in Fig. 4 (top panel, solid line). The modulus of the resulting Fourier transform is shown in Fig. 4 (bottom panel). In order to extract structural parameters of interest, the first three shells are Fourier filtered and then backtransformed and the contribution from these components is modeled. Because of the weak backscattering amplitude of hydrogen, the Si-H distance is not included in any fit, but Si-O and Si-Cl distances are included as appropriate. Each shell is first modeled independently and then the three are modeled together until the best fit to the data is found. This three-shell fit is then plotted as a dashed line with the EXAFS and the Fourier transform in Fig. 4. It is also emphasized that for the surface data the only amplitude parameters varied in these and subsequent fits were the effective coordination numbers. All other parameters (mean free path of the photoelectrons, Debye-Waller-like factor) were those derived from the model compound bulk Si data [this is similar to the procedure followed by Jaeger *et al.* in the O-Mo(100) work[6]]. While surface mean-free-path and Debye-Waller-like parameters may be different from bulk values[44,45] and their variation would undoubtedly produce better fits, allowing these to vary as free parameters along with the coordination numbers would produce a result which could not be easily interpreted. Error bars in the distance determinations were

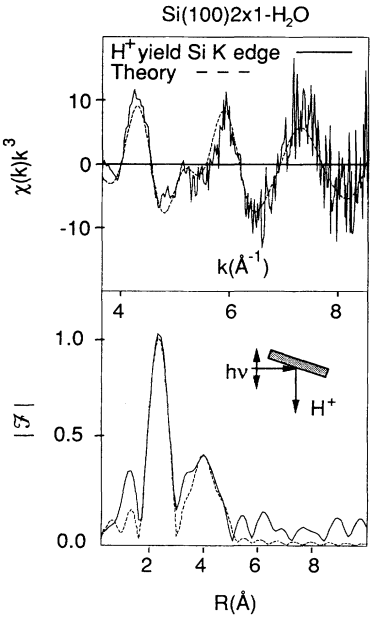

FIG. 4. Top panel: H^+ yield EXAFS data above the Si K edge for 0.5 ML of H_2O on Si(100)2×1 after background subtraction and normalization to the edge jump [corresponding to the data in Fig. 3 (b)]. The EXAFS function $\chi(k)$ weighted by k^3 (solid line) and the best theoretical three-shell fit (dashed line) are compared. Bottom panel: the Fourier transform $\mathcal{F}$ of the EXAFS shown above together with the best three-shell fit.

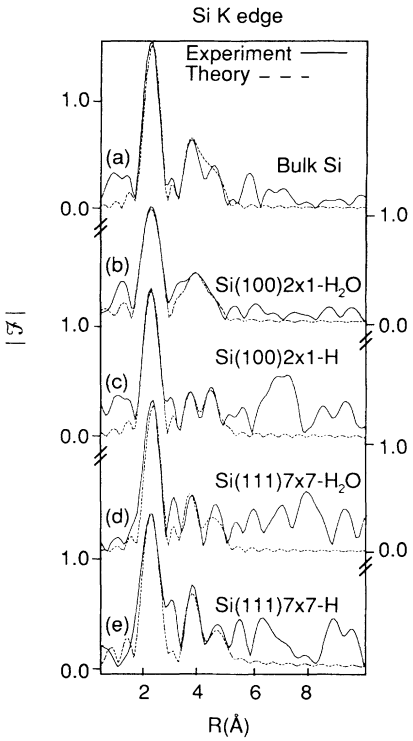

FIG. 5. Fourier transforms $\mathcal{F}$ of the background subtracted edge-height normalized EXAFS $\chi(k)$ corresponding to Figs. 3(a)–3(e) (solid lines), together with the best theoretical three-shell fits (dashed lines). The bulk Si spectrum was recorded by monitoring total electron yield, while the others represent the H^+ yield.

estimated by studying the changes in distance introduced by varying the threshold energy E_0 and by taking different k-space ranges for the data. The error bars in the coordination numbers were taken to be ±20%.

In order to reduce unnecessary length, only the moduli of the Fourier transforms and the corresponding fit will subsequently be shown. Figure 5(a) shows the Fourier transform and fit from bulk Si corresponding to the data of Fig. 3(a). Three shells of atoms are clearly visible corresponding to distances of 2.35, 3.84, and 4.5 Å and to coordination numbers of 4, 12, and 12, respectively. We now present the results for the ion yield and AEY studies.

1. Si(100)2×1-H_2O

Figure 4 shows the EXAFS and the Fourier transform from Si(100)2×1-H_2O; the Fourier transform is repeated in Fig. 5(b) for completeness. After phase-shift correction the distances for the first three nearest-neighbor shells are found to be 2.37±0.02, 3.9±0.1, and 4.6±0.2 Å. The coordination numbers for each shell in this experimental geometry were 3.1, 10.7, and 8.5, respectively. These results are listed in Table I, row 1.

In order to evaluate these data further, we have performed calculations of the bond lengths and effective coordination numbers for a model adsorption site, using the methodology described above. The Si(100)2×1 sur-

TABLE I. Results of the three-shell fits to the ion yield Si *K*-edge data. The errors quoted are estimated from the results of several analyses of each spectrum, where different background subtraction, Fourier windows, data ranges, etc., were employed. The figures for bulk Si are from Ref. 62.

	Average distance in Å			Effective coordination nos.		
	R_1	R_2	R_3	N_1	N_2	N_3
Si(100)2×1-H_2O	2.37	3.90	4.6	3.1	10.7	8.5
Si(100)2×1-H	2.36	3.82	4.5	3.5	5.5	12.5
Si(111)7×7-H_2O	2.35	3.80	4.5	3.7	8.6	12
Si(111)7×7-H	2.34	3.86	4.6	4.1	14	12
Si(100)2×1-Cl	2.36	3.87	4.4	3.7	14	3
Si(111)7×7-Cl	2.34	3.82	4.5	3.3	9.6	9.7
Bulk Si	2.35	3.84	4.5	4	12	12
Estimated error	±0.02	±0.1	±0.2	±1	±3	±4

face has been studied using a wide variety of structural and modeling techniques. This 2×1 structure is interpreted as being due to the formation of dimers at the surface. Scanning tunneling microscopy[46–48] (STM) indicates the presence of roughly equal numbers of nonbuckled and buckled dimers, together with dimer-vacancy defects. Several studies indicate dissociative adsorption at room temperature, with some rotational freedom from the OH and H bonded to the Si dimer atoms.[8,27] The Si(100)2×1-H_2O calculations were averaged over both domains on the Si surface, and in agreement with the STM results, over both symmetric and asymmetric dimer types. The dimer models used were the Levine[49] (symmetric) and Chadi[50,51] (asymmetric) models. The Chadi model was chosen as it seems to be favored by many of the experimental studies.[52] The asymmetric dimer models indicate a charge transfer to the "upper" atom of the dimer.[53] The high electron density should favor bonding to H, with OH bonded to the lower, electron-deficient site. Therefore selective bonding of H to the upper atom of the dimer was chosen in the case of asymmetric dimers. An O atom bonded to the other Si dimer atom was included in the second shell of neighboring atoms.

On the basis of the above model, the first three shells lies at bond lengths of 2.37, 3.69, and 4.5 Å, the corresponding effective coordination numbers being 1.92, 7.9, and 3.9, respectively. These are listed in Table II, row 1. To evaluate whether the ion yield originates from surface or bulk processes, the calculations can be compared with the experimentally derived values and the bulk figures of 2.35, 3.84, and 4.5 Å and 4, 12, and 12 nearest-neighbor atoms. The first-shell data are the most accurately known, and here the surface and bulk experimental values and the measured value for the bond length all lie within the experimental error of each other; the effective coordination number lies marginally closer to that of the bulk value. For the second shell, the bond length and coordination number lie within experimental error of the bulk value and outside the calculated surface values, and for the third shell, the margin of error includes both surface and bulk models. In terms of choosing between surface and bulk origin therefore the strongest evidence comes from the second-shell data which indicate a bulk origin.

2. *Si(100)2×1-H*

The modulus of the Fourier transform corresponding to the EXAFS from Si(100)2×1-H is shown in Fig. 5(c). While the noise in the spectrum produces extra components below 2 Å and above 5 Å, the three shells of data can clearly be seen. The best three-shell fit to the data is shown by the dashed line. The three shells have bond lengths of 2.36±0.02, 3.82±0.1, and 4.5±0.2 Å and effective coordination numbers of 3.5±1, 5.5±3, and 12.5±4, respectively. The model calculations of distances and effective coordination number in this case were based on the experimental geometry proposed by Schaefer *et al.*[30] This has H adsorbed on both atoms of the Si-Si dimer. Thus the information from the H^+ yield in this case should be an average of three adsorption sites: the symmetric dimer site and the upper and lower atoms of the asymmetric dimers, with additional averaging over both domains present. The results are shown in Table II, row 2. The first three shell distances are 2.37, 3.70, and 4.5 Å. Compared with the experimental values obtained above, the first- and third-shell distances are consistent with both a surface and bulk origin, while the second-shell distance can only be explained in terms of a bulk origin. The coordination numbers for the first and third shell both indicate a bulk origin, that for the second shell is closer to the surface calculation.

3. *Si(111)7×7-H_2O*

Figure 5(d) shows the Fourier transform corresponding to the EXAFS from Si(111)7×7-H_2O recorded in H^+ yield. The data are noisy, producing transform components above 5 Å and below 2 Å and a component at ~3 Å. The component at ~3 Å has not been fitted as it falls in a place where neither a surface or bulk peak is expected. The data are modeled with a three shell fit, and the best fit is shown as the dashed line in Fig. 5(d). The

TABLE II. Calculated coordination numbers and average bond lengths expected at the Si K edge for the systems studied and the experimental geometries employed, based on the structural models described in the text. For bulk Si the effective coordination numbers equal the actual coordination numbers as expected.

	Average distance in Å			Effective coordination nos.		
	R_1	R_2	R_3	N_1	N_2	N_3
Si(100)2×1-H_2O	2.37	3.69	4.5	1.92	7.9	3.9
Si(100)2×1-H	2.37	3.70	4.5	1.75	6.7	3.6
Si(111)7×7-H_2O	2.35	3.84	4.5	1.3	6.4	8.4
Si(111)7×7-H	2.35	3.84	4.5	1.3	6.4	8.4
Si(100)2×1-Cl	2.11	3.72	4.5	3.5	7.0	3.6
Si(111)7×7-Cl	2.15	3.84	4.5	4.4	6.4	8.4
Bulk Si	2.35	3.84	4.5	4	12	12

distances measured were 2.35±0.02 3.80±0.1, and 4.5±0.2 Å and the corresponding effective coordination numbers were 3.7±1, 8.6±3, and 12±4.

To model the surface distances and effective coordination numbers, the known adsorption geometry for H_2O on Si(111)7×7 was utilized. The Si(111)7×7 surface structure is taken to be the dimer-adatom-stacking-fault model.[54] These surfaces form the substrates for the adsorption systems studied. All results indicate a dissociative adsorption mode in the temperature range 80–400 K.[30–32] For Si(111)7×7-H_2O and Si(111)7×7-H_2, an atop adatom site was assumed, the adatom being bonded to three Si atoms below it. This is consistent with recent STM results.[32] This approximation has been used before in other such calculations on the Si(111)7×7 surface.[43,55] This model for the H adsorption site has Si backscattering shells about the Si adatom at distances of 2.35, 3.84, and 4.5 Å, i.e., bulk values, and the effective coordination numbers are 1.3, 6.4, and 8.4, respectively. (The results are identical for both the H_2O- and H_2-dosed surfaces.) The results for this surface are shown in Table II, row 3; the first shell distance of 2.35 Å produces an effective coordination number of 1.3, whereas the measured value is 3.7, close to the bulk value of 4. The higher shell coordination numbers and distances are all consistent with the bulk values and not with the surface values.

4. *Si(111)7×7-H*

Figure 5(e) shows the Fourier transform corresponding to the EXAFS from this system. The dashed line indicates the best three-shell fit to these data. The nearest-neighbor distances are 2.34±0.02, 3.86±0.1, and 4.6±0.2 Å; the corresponding effective coordination numbers are 4.1±1, 14±3, and 12±4, respectively. An appropriate model calculation was based on the model of the monohydride phase. The calculation gives effective coordination number of 1.3, 6.4, and 8.4, which is not consistent with the measured value. The measured values are all closer to the bulk values in this system.

5. *Si(111)7×7-H_2O and Si(111)7×7-H NEXAFS*

Figure 6 shows the NEXAFS spectra of bulk silicon in total electron yield, together with H^+-ion yield NEXAFS for the Si(111)7×7-H_2O and Si(111)7×7-H systems. The spectra are all very similar in shape at the edge and there is no edge shift evident which might reflect a different final state for the photoemitted electrons. This result may be contrasted with those of Rosenberg *et al.*[7], who recorded H^+ and D^+ yield spectra from the Si(111)7×7-H_2O and Si(111)7×7-D_2O systems at the Si $L_{2,3}$ edge (~100 eV). In that case a shift of 0.5 eV was observed between the ion yield and the TEY spectra. No corresponding shift is evident in our K-edge data; such a shift, however, might be obscured because of the poorer resolution of the double crystal monochromator (~2 eV) at the Si K edge. Although the similarity in Fig. 6 might suggest an XESD mechanism, it is not clear (in the absence of calculations) whether NEXAFS data from a H or H_2O adsorbate surface would be expected to differ substantially from the bulk NEXAFS at this edge. This evidence must be considered inconclusive.

6. *Si(100)2×1-Cl*

The Fourier transform corresponding to the EXAFS from bulk Si is reproduced from Fig. 5(a) in Fig. 7(a) for

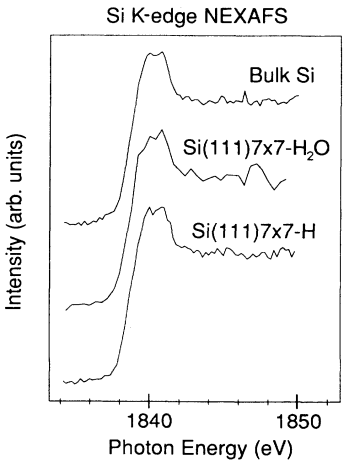

FIG 6. Comparison of Si K-edge NEXAFS. The bulk Si spectrum was taken in total electron yield, while the others were H^+ yield. The step width was 0.5 eV in each case.

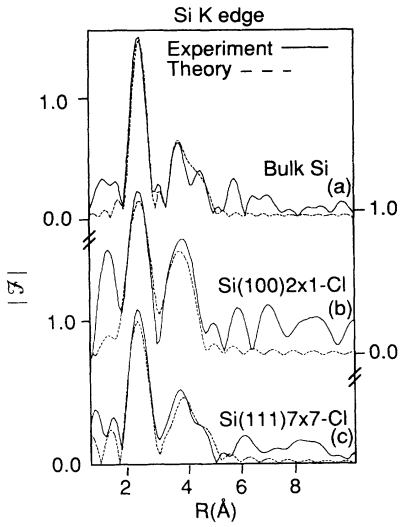

FIG. 7. Fourier transforms $\mathcal{F}$ of the background subtracted edge height normalized EXAFS $\chi(k)$ together with the best theoretical three-shell fits (dashed lines), corresponding to Figs. 3(a), 3(f), and 3(g). The bulk Si spectrum was recorded by monitoring total electron yield, while the other spectra are Cl^+-ion yield data.

comparison with the other data presented in this figure. Figure 7(b) shows the Fourier transform corresponding to the background subtracted and normalized EXAFS from the Si(100)2×1-Cl system [from Fig. 3(f)]. The signal-to-noise ratio in the data is poor in comparison with the other spectra shown; nevertheless, the Fourier transform of the data reveals a first-shell component and a mixture of second and third shells. The discrepancy in the second and third shells in the case of Si(100)2×1-Cl is noteworthy. The presence of a glitch in the data at ~200 eV (~7 $Å^{-1}$) above the edge due to a Bragg peak in the InSb(111) monochromator crystals which is not entirely normalized out in the ion-yield data seems to have caused this distortion in the higher shells. The spectrum was analyzed with and without this glitch, and the first shell results were found to be reproducible, whereas large variations in the higher shells occurred. The component at the unphysical distance of ~1 Å can be attributed to low-frequency noise and is most likely due to imperfect background subtraction giving a residual long-period oscillation under the EXAFS. An attempt was made to fit the first shell data with Si-Si and Si-Cl backscatterers; however, the Si-Cl component was rejected in the least-squares fitting procedure. A three-shell fit to the data gives bond lengths of 2.36±0.02, 3.87±0.1, and 4.4±0.2 Å and effective coordination numbers of 3.7±1, 14±3, and 3±4, respectively.

The model calculations for this system are based on the dimer adsorption site determined geometry from photoemission measurements[33] and from SEXAFS.[34,37,38] The SEXAFS bond length is 2.01±0.02 Å. For Si(100)2×1-Cl, a scheme similar to that employed for Si(100)2×1-H was used. The first shell is a weighted average of contributions from three Si and one Cl backscattering atoms. The results of these calculations are given in Table II, row 5. The bond lengths predicted are 2.11, 3.72, and 4.5 Å and the corresponding effective coordination numbers are 3.5, 7.0, and 3.6, respectively. The first-shell comparison provides a clear test of a system where it is known that a different bond length should result if the measurements were surface sensitive. This is not the case and provides a strong indication of a bulk origin for these data.

7. *Si(111)7×7-Cl*

Figure 7(c) shows the Fourier transform corresponding to the Cl^+-ion yield data of Fig. 3(g). The Fourier transform reveals a strong first shell peak and a mixture of two higher shells in the region 2–5 Å. The modeling of these data is shown with the dashed line. The model is based on shells of Si backscatterers. An attempt was made to fit the data to a Cl-Si bond length of 2.0 Å, based on the Auger SEXAFS results described below. However, this led to an increased fit index indicating a worse fit. This is strong evidence that the ion yield has a bulk origin and is substantiated by the higher-shell data and calculations. The results of the three shell fit are bond lengths of 2.34±0.02, 3.82±0.1, and 4.5±0.2 Å with effective coordination numbers of 3.3±1, 9.6±3 and 9.7±4, respectively. These are recorded in Table I, row 6.

The structure of Si(111)7×7-Cl is known from previous results. On Si(111)7×7, after room-temperature exposure, photoemission shows evidence for a number of inequivalent sites.[33] A SEXAFS investigation has shown that after annealing the dosed surface to 400 °C, the Cl adatoms occupy atop sites with a first nearest-neighbor bond length of 2.03±0.03 Å.[35] Photoemission results confirm this adsorption site geometry for this phase.[36] NEXAFS from annealed Si(111)7×7-Cl displays two resonances which are interpreted in terms of transitions into the antibonding (Cl,Si) 3*p*-derived σ_z states and antibonding $\pi_{x,y}$ states. The Cl-Si bond length in this system is again much shorter than the Si-Si bond length of 2.35 Å and this difference should allow the true PSID-KF contribution to be distinguished for Cl^+-ion yield at the Si *K* edge. Calculated bond lengths for this model were 2.15, 3.84, and 4.5 Å with coordination numbers of 4.4, 6.4, and 8.4, respectively. These results are clearly not consistent with the experimental data, which are much closer to values for the bulk.

B. Cl *K*-edge measurements

Figure 8 shows EXAFS spectra recorded in AEY and Cl^+-ion yield mode at and above the Cl *K* edge at the same grazing angle. The top panel is for the Si(100)2×1-Cl system and the bottom panel shows results of the Si(111)7×7-Cl system. Tick marks are provided over the main spectral features as a guide to the eye. The correspondence of the main features indicates that the dominant scattering distance (the Si-Cl bond length) is similar in each of these systems.

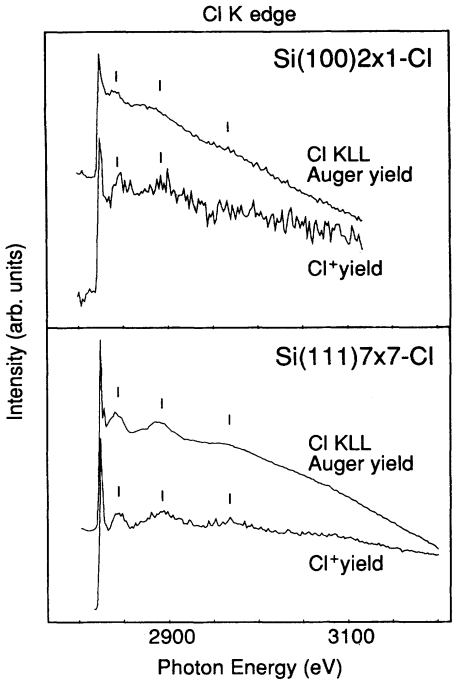

FIG. 8. Top panel: comparison of Cl K-edge SEXAFS for Cl^+-ion yield and Auger electron yield for the Si(100)2×1-Cl system at room temperature. Bottom panel: comparison of the Cl K-edge SEXAFS for Cl^+-ion yield and AEY in the Si(111)7×7-Cl system. The tick marks are provided as a guide to the eye.

1. *Si(100)2×1-Cl*

The spectra in the top panel of Fig. 8 represent AEY spectra and Cl^+-ion yield from the system. The analysis of the AEY data (not shown) indicates that the spectrum is dominated by a first shell. The bond length, from these and other data,[34,37,38] is 2.01±0.02 Å. The poor quality of the Cl^+-ion yield data from this system precluded an EXAFS analysis, but qualitatively the spectrum is similar to that of the Auger yield data; the fact that any edge jump is measured in ion yield at the adsorbate edge means that there is some correlation between the absorption event at the surface and the ion desorption.

The correspondence between ion yield and Auger yield is also found in the NEXAFS spectra shown in Fig. 9. An ion-yield spectrum at 15° grazing angle is compared with Auger yield spectra at 15°, 40°, and 75°. Clearly, the agreement between the measurement modes is only observed at equivalent incidence angles.

2. *Si(111)7×7-Cl*

Finally, we compare ion and Auger electron yield spectra from Si(111)7×7-Cl. The raw data are presented in Fig. 8, bottom panel. The spectra are qualitatively very similar. The Fourier transform of the Auger yield spectra [Fig. 10(a)] is dominated by the first shell of Cl-Si backscattering. The Cl-Si bond length is 2.00±0.02 Å,

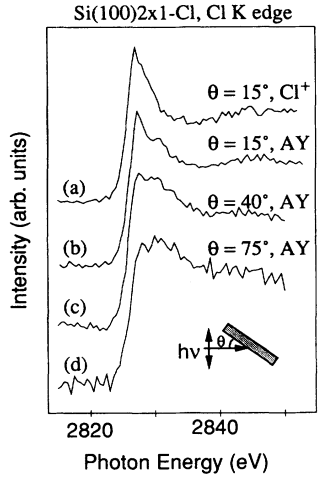

FIG. 9. Comparison of room-temperature Cl K-edge NEXAFS for the Si(100)2×1-Cl system from Cl^+-ion yield and Cl *KLL* Auger yield.

and no EXAFS oscillations were evident in the normal incidence geometry, in agreement with the previous measurements[35] from this system. The Cl-Si bond distance is the same, within error bars, as that obtained in this earlier work (2.03±0.03 Å). Our data are consistent with the lower limit of ~75% occupation of the atop geometry site given by Citrin, Rowe, and Eisenberger,[35] based on the absolute amplitude of their grazing incidence SEXAFS data.

The Fourier transform of the Si(111)7×7-Cl Cl^+-ion yield data is shown in Fig. 10(b). These data, though poorer in signal-to-noise ratio than the AEY data, are again dominated by a first neighbor distance of 2.00±0.02 Å, identical to that recorded in AEY. Additionally, the similarity of the effective co-ordination numbers (PSID, 2.9±0.7; AEY, 2.1±0.7) points to the Cl^+ yield being a monitor of the surface absorption coefficient

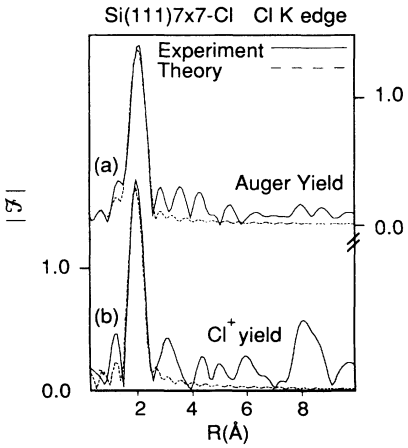

FIG. 10. Fourier transforms $\mathcal{F}$ of the background subtracted edge height normalized EXAFS $\chi(k)$ together with the best theoretical single-shell fits (dashed lines), corresponding to Fig. 8 bottom panel.

in this case. The fact that the PSID and AEY results are so similar rules out the possibility that the Cl^+ ions are desorbing from minority sites with a more favorable desorption cross section.

IV. DISCUSSION

The main aim of this paper is to determine the origin of the x-ray absorption fine structure in the ion yield at the substrate edge for a range of silicon adsorbate systems. If the EXAFS and NEXAFS information matches the known local geometry of the substrate Si atom, a KF mechanism may be inferred for the PSID. If the information mirrors the bulk geometry, the implication is that XESD dominates. A secondary issue is the ion-yield mechanism which operates at the Cl adsorbate edge.

A. Substrate edge PSID

The results presented in the preceding section can now be summarized in these terms. In the four H^+ studies of H_2 and H_2O adsorption the adsorbate atoms are not "visible" in the sense discussed above: hydrogen is a very weak scatterer while oxygen in these cases is confined to the second shell. The discussion then turns on the less obvious differences between the substrate surface structure and that of the bulk. In these four cases the first-neighbor bond length is consistent with either surface or bulk values. However, the coordination numbers in the first shell are consistent only with the bulk data and, taken together, the first shell results therefore point to a bulk origin for these EXAFS. The second shell data are consistent in two cases [Si(100)2×1-H and Si(111)7×7-H_2O] with surface values only, in three cases with the bulk values only and in one case with both surface and bulk values. The third-shell data are consistent in five cases with bulk values only, in one case with surface values only. Though not as reliable a test as the first-shell data, the higher-shell data generally support the view that the origin of the EXAFS at the substrate edge is bulk.

In our earlier analysis of the Si(100)2×1-H_2O system, we assumed that a difference between the edge jumps in PSID and TEY was evidence for a dominance of KF over XESD.[17] Following questioning of this criterion by Menzel,[18] we showed that this indeed ignores cross-section effects which prevent the XESD yield being simply equated with TEY.[19] A more valid approach to distinguish between the KF and XESD mechanisms is the one discussed in the preceding paragraph.

A more definitive test arises with the first shell in the Si(100)2×1-Cl and Si(111)7×7-Cl systems. This is because the adsorbate chlorine should be clearly visible as a backscattering atom[23] at a significantly different bond distance.[37,38] In both cases, the grazing incidence geometry employed should favor the Si-Cl bond direction, as this bond lies close to the surface normal. This is reflected in the calculated "effective" R values of 2.11 and 2.15 Å, which are weighted averages of a Si-Cl bond and three Si-Si bonds. However, the experimentally determined first-shell values of 2.36 and 2.34±0.02 Å are within experimental error equal to that of bulk Si. Any attempt to fit a Si-Cl shell was rejected in the least-squares-fitting procedure. The clear conclusion is that PSID from these systems at the substrate edge has a bulk origin. It is worth noting that the effective coordination numbers in this shell do not allow a clear distinction between bulk and surface. The scattering distances in the other two shells are also inconclusive, but the experimental effective coordination number in the second shell is clearly bulklike.

It is instructive to compare these results with the original PSID SEXAFS experiment of Jaeger *et al.*:[6] in that experiment the adsorbate oxygen was not distinguished due to $L_{2,3}$ EXAFS overlapping the low-k range of the data where the oxygen backscattering is significant. The resulting first-shell scattering length was indistinguishable from that of the bulk so that the surface character could only be confirmed from the reduced effective coordination number. The normalization of the amplitude was made rather difficult by the presence of glitches at the edge.

The conclusion of the O-Mo experiment was that the minority-site α-oxygen phase desorbs from an unreconstructed part of the Mo surface. However, there is some evidence that the adsorbate-covered surface is strongly reconstructed. The α-oxygen phase under study by Jaeger *et al.*[6] was formed by dosing with 100-L O_2; the terminology comes from ESD studies on polycrystalline Mo where two desorption thresholds were identified. The β phase has a vanishingly small ESD cross section and forms at low coverages and low-dose conditions at room temperature. It has an adsorption energy of 100–120 kcal/mole.[56,57] The α phase forms at higher coverages and has a very high desorption yield and a smaller adsorption energy [37–60 kcal/mol (Refs. 56 and 57)]. The desorption cross section for the α phase is $\sim 10^4$ greater than for the β phase.[58] Studies involving both ESD and LEED allow the classification of the α phase in terms of coverage and LEED patterns. Yu[58] determines the onset of the α phase after 3.5-L exposure; the LEED pattern is initially 1×1 and changes to a $p(1\times1)$ at saturation. Bauer and Poppa[59] also identify this very high yield ESD state at higher coverages. The LEED pattern for this phase is a diffuse 1×1. This study and other LEED and work-function studies[60,61] suggest that the Mo surface is strongly reconstructed in this coverage range, with the formation of a surface oxide phase. To reconcile the PSID conclusion that the α-oxygen desorbs from bulklike metal sites, it is necessary to infer that in the presence of the surface oxide there are still parts of the surface which are unreconstructed. It is suggested that a full structural study of the α and β phases is needed to clarify this point.

B. Adsorbate edge PSID

There is clear evidence for the dominance of a surface desorption mechanism in the measurements of Cl^+ yield EXAFS at the Cl K edge presented in Fig. 8. The ab-

sorption threshold is the same for the Auger yield and ion-yield data, ruling out multielectron excitations as the cause of desorption. There is a good correspondence between the spectral features observed in both measurement techniques, even in the rather ion-yield SEXAFS data for Si(100)2×1-Cl. The NEXAFS data of Fig. 9 also correspond well, with the same main "white line" at ~2825 eV and the broad feature centered at ~2845 eV in each. The analysis of the ion-yield SEXAFS from Si(111)7×7-Cl provides quantitative evidence that the information has a surface origin.

The two possible mechanisms to explain this surface origin are KF and ESD by electrons arising from the absorption events in neighboring Cl atoms. Both mechanisms should provide true SEXAFS information. It is difficult to formally distinguish between these two mechanisms. Because ESD cross sections are not well known, the comparison of the PSID edge jump with that of TEY or even AEY will not be definitive. The limitation of this approach for a *substrate* edge has already been discussed.[19] However, the very large difference between the edge jump in TEY (1–2%) and Cl^+ yield (>200%) at this *adsorbate* edge would seem to indicate that the desorption is dominated by the KF mechanism. While these data show that ion desorption can provide surface EXAFS information at an adsorbate edge, it seems unlikely that this detection mechanism will supplant the established Auger electron, total electron, or fluorescence yield techniques, except in specific cases where the latter are limited in scope.

V. CONCLUSIONS

The measurements on silicon adsorbate systems presented in this paper are a significant increase in the data base of PSID EXAFS. From our data we can conclude the following.

(a) At the substrate Si *K* edge, the characteristic parameters are closer to bulk than to surface values indicating that the dominant desorption mechanism is not KF but XESD. Especially relevant is lack of a distinct Si-Cl first shell, chlorine being a "visible" adsorbate whose amplitude should be favored by the experimental geometry. By comparison with these systems, there seems to be a case for reexamination of the Mo(100)-O system,[6] specifically an investigation of the surface structure by other techniques. A scanning tunneling microscopy study would be particularly helpful in this respect.

(b) At the adsorbate Cl *K* edge, the ion-yield EXAFS contains information related to the surface absorption events. The NEXAFS data also correspond well with the Auger yield. The most likely mechanism is the KF mechanism. However, this opens up only limited possibilities for SEXAFS measurements: the same information can usually be obtained with other, well-established methods.

ACKNOWLEDGMENTS

This work was supported by the United Kingdom Science and Engineering Research Council with additional support from Johnson Matthey. Useful discussions with D. P. Woodruff are acknowledged.

[1]For reviews see P. H. Citrin, J. Phys. (Paris) Colloq. **47**, C8-437 (1986); J. Stöhr, in *X-Ray Absorption: Principles, Applications, Techniques* of *EXAFS, SEXAFS and XANES,* edited by R. Prins and D. Konigsberger (Wiley, New York, 1988).

[2]F. Comin, L. Incoccia, P. Lagarde, G. Rossi, and P. H. Citrin, Phys. Rev. Lett. **54**, 122 (1985).

[3]M. Knotek and P. J. Feibelman, Phys. Rev. Lett. **40**, 964 (1978).

[4]M. Knotek, Rep. Prog. Phys. **47**, 1499 (1984).

[5]D. Norman, J. Phys. C **19**, 3273 (1986).

[6]R. Jaeger, J. Feldhaus, J. Haase, J. Stöhr, Z. Hussain, D. Menzel, and D. Norman, Phys. Rev. Lett. **45**, 1870 (1980).

[7]R. A. Rosenberg, P. J. Love, V. Rehn, I. Owen, and G. Thornton, J. Vac. Sci. Technol. A **4**, 1451 (1986).

[8]C. U. S. Larsson, A. S. Flodström, R. Nyholm, L. Incoccia, and L. Senf, J. Vac. Sci. Technol. A **5**, 3321 (1987).

[9]J. A. Yarmoff, A. Taleb-Ibrahimi, F. R. McFeely, and Ph. Avouris, Phys. Rev. Lett. **60**, 960 (1988).

[10]J. A. Yarmoff and S. A. Joyce, Phys. Rev. B **40**, 3143 (1989).

[11]For a recent review see R. D. Ramsier and J. T. Yates, Jr., Surf. Sci. Rep. **12**, 243 (1991).

[12]R. Jaeger, J. Stöhr, and T. Kendelewicz, Phys. Rev. B **28**, 1145 (1983).

[13]R. Jaeger, J. Stöhr, and T. Kendelewicz, Surf. Sci. **134**, 547 (1983).

[14]J. Schmidt-May, F. Senf, J. Voss, C. Kunz, A. Flodström, R. Nyholm, and R. Stockbauer, Surf. Sci. **163**, 303 (1985).

[15]I. W. Owen, N. B. Brookes, C. H. Richardson, D. R. Warburton, F. M. Quinn, D. Norman, and G. Thornton, Surf. Sci. **178**, 897 (1986).

[16]D. E. Ramaker, T. E. Madey, R. L. Kurtz, and H. Sambe, Phys. Rev. B **38**, 2099 (1988); also V. Rehn and R. A. Rosenberg, Phys. Rev. B **40**, 6436 (1989).

[17]R. McGrath, I. T. McGovern, D. R. Warburton, G. Thornton, and D. Norman, Surf. Sci. **178**, 101 (1986).

[18]D. Menzel, in *The Structure of Surfaces II: Proceedings of the Second International Conference on the Structure of Surfaces,* edited by J. F. van der Veen and M. A. Van Hove (Springer-Verlag, Berlin, 1988), p. 65.

[19]R. McGrath, I. T. McGovern, D. R. Warburton, G. Thornton, D. Norman, and R. Cimino, Vacuum **38**, 424 (1988).

[20]R. Treichler, W. Riedl, W. Wurth, P. Feulner, and D. Menzel, Phys. Rev. Lett. **54**, 462 (1985).

[21]R. Jaeger, J. Stöhr, R. Treichler, and K. Baberschke, Phys. Rev. Lett. **47**, 1399 (1981).

[22]R. Jaeger, R. Treichler, and J. Stöhr, Surf. Sci. **117**, 533 (1982).

[23]B. K. Teo and P. A. Lee, J. Am. Chem. Soc. **101**, 2815 (1979).

[24]The data from this system have been presented in a preliminary report to a conference proceedings, D. Purdie, C. A. Muryn, N. S. Prakash, P. L. Wincott, G. Thornton, and D. S.-L. Law, Surf. Sci. **251/252**, 546 (1991).

[25]P. A. Thiel and T. E. Madey, Surf. Sci. Rep. **7**, 211 (1987).

[26]R. McGrath, I. T. McGovern, D. R. Warburton, G. Thornton, D. Norman, and R. Cimino, Vacuum **38**, 251 (1988).

[27]A. L. Johnson, M. M. Walczak, and T. E. Madey, Langmuir

4, 277 (1988).
[28]J. A. Schaefer, J. Anderson, and G. J. Lapeyre, J. Vac. Sci. Technol. A **3**, 1443 (1985).
[29]J. A. Schaefer, Surf. Sci. **178**, 90 (1986).
[30]J. A. Schaefer, F. Stucki, W. Göpel, and G. J. Lapeyre, J. Vac. Sci. Technol. B **2**, 359 (1984).
[31]H. Froitzheim, U. Köhler, and H. Lammering, Surf. Sci. **149**, 537 (1985).
[32]Ph. Avouris and I.-W. Lo, Surf. Sci. **242**, 1 (1991).
[33]J. E. Rowe, G. Margaritondo, and S. B. Christman, Phys. Rev. B **16**, 1581 (1977).
[34]G. Thornton, P. L. Wincott, R. McGrath, I. T. McGovern, F. M. Quinn, D. Norman, and D. D. Vvedensky, Surf. Sci. **211/212**, 959 (1989).
[35]P. H. Citrin, J. E. Rowe, and P. Eisenberger, Phys. Rev. B **28**, 2299 (1983).
[36]R. D. Schnell, D. Rieger, A. Bogen, F. J. Himpsel, K. Wandelt, and W. Steinmann, Phys. Rev. B **32**, 8057 (1985).
[37]D. Purdie, C. A. Muryn, N. S. Prakash, K. G. Purcell, P. L. Wincott, G. Thornton, and D. S.-L. Law, in *X-Ray Absorption Fine Structure,* edited by S. Hasnain (Horwood, Chichester, 1991), p. 206.
[38]D. Purdie, C. A. Muryn, N. S. Prakash, K. G. Purcell, P. L. Wincott, G. Thornton, and D.S.-L. Law, J. Phys. Condens. Matter **3**, 7751 (1991).
[39]N. D. Spenser, P. J. Goddard, P. W. Davies, M. Kitson, and R. M. Lambert, J. Vac. Sci. Technol. A **1**, 1554 (1988). The Cl source is a modified version of the design described in this work.
[40]A. A. MacDowell, D. Norman, and J. B. West, Rev. Sci. Instrum. **57**, 2667 (1986).
[41]S. J. Gurman, N. Binsted, and I. Ross, J. Phys. C **17**, 143 (1984).
[42]G. Thornton and W. Myring (unpublished).
[43]P. H. Citrin, P. Eisenberger, and J. E. Rowe, Phys. Rev. Lett. **48**, 802 (1982).
[44]F. Sette, C. T. Chen, J. E. Rowe, and P. H. Citrin, Phys. Rev. Lett. **59**, 311 (1988); **60**, 2098 (1988); D. Chandesris and G. Rossi, *ibid.*, **60**, 2097 (1988).
[45]M. Bader, A. Puschmann, C. Ocal, and J. Haase, Phys. Rev. Lett. **57**, 3273 (1986).
[46]R. M. Tromp, R. J. Hamers, and J. E. Demuth, Phys. Rev. Lett. **55**, 1303 (1985).
[47]R. M. Tromp, R. J. Hamers, and J. E. Demuth, Phys. Rev. B **34**, 1388 (1986).
[48]R. J. Hamers, R. M. Tromp, and J. E. Demuth, Phys. Rev. B **34**, 5343 (1986).
[49]J. D. Levine, Surf. Sci. **34**, 90 (1973).
[50]D. J. Chadi, Phys. Rev. Lett. **43**, 43 (1979).
[51]D. J. Chadi, J. Vac. Sci. Technol. **16**, 1290 (1979).
[52]P. J. Dobson, in *Properties of Silicon: EMIS Datareviews Series No. 4* (Inspec, London, 1988), p. 849.
[53]See, e.g., G. K. Wertheim, D. M. Riffe, J. E. Rowe, and P. H. Citrin, Phys. Rev. Lett. **67**, 120 (1991).
[54]K. Takayanagi, Y. Tanishiro, S. Takahashi, and M. Takahashi, Surf. Sci. **164**, 367 (1985).
[55]S. J. Morgan, A. R. Law, R. H. Williams, D. Norman, R. McGrath, and I. T. McGovern, Surf. Sci. **204**, 428 (1988).
[56]P. H. Dawson, Phys. Rev. B **15**, 5522 (1977).
[57]P. A. Redhead, Can. J. Phys. **42**, 886 (1964).
[58]M. L. Yu, Phys. Rev. B **19**, 5995 (1979).
[59]E. Bauer and H. Poppa, Surf. Sci. **88**, 31 (1979).
[60]R. Riwan, C. Guillot, and J. Paigne, Surf. Sci. **47**, 183 (1975).
[61]E. I. Ko and R. J. Madix, Surf. Sci. **109**, 221 (1981).
[62]R. W. G. Wyckoff, *Crystal Structures,* 2nd ed. (Krieger, Malabar, FL, 1982).

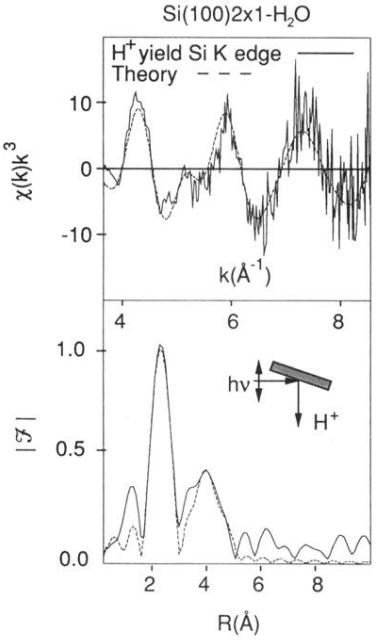

FIG. 4. Top panel: H^+ yield EXAFS data above the Si K edge for 0.5 ML of H_2O on Si(100)2×1 after background subtraction and normalization to the edge jump [corresponding to the data in Fig. 3 (b)]. The EXAFS function $\chi(k)$ weighted by k^3 (solid line) and the best theoretical three-shell fit (dashed line) are compared. Bottom panel: the Fourier transform $\mathcal{F}$ of the EXAFS shown above together with the best three-shell fit.

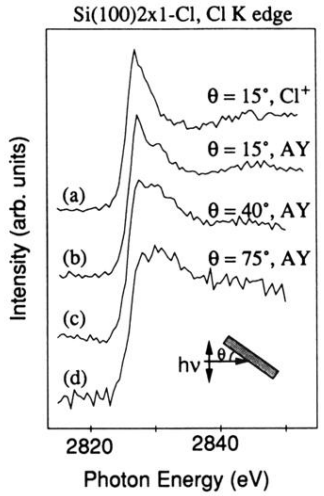

FIG. 9. Comparison of room-temperature Cl *K*-edge NEXAFS for the Si(100)2×1-Cl system from Cl^+-ion yield and Cl *KLL* Auger yield.